

# Modulation of unpolarized light in planar aligned subwavelength-pitch deformed-helix ferroelectric liquid crystals

Vladimir V. Kesaev,<sup>1,\*</sup> Evgeny P. Pozhidaev,<sup>1,†</sup> and Alexei D. Kiselev<sup>2,‡</sup>

<sup>1</sup>*Lebedev Physical Institute, Leninsky Prospekt 53, 119991 Moscow, Russia*

<sup>2</sup>*Saint Petersburg National Research University of Information Technologies,*

*Mechanics and Optics (ITMO University), Kronversky Prospekt 49, 197101 Saint Petersburg, Russia*

(Dated: September 4, 2022)

We study the electro-optic properties of subwavelength-pitch deformed-helix ferroelectric liquid crystals (DHFLC) illuminated with unpolarized light. In the experimental setup based on the Mach-Zehnder interferometer, it was observed that the reference and the sample beams being both unpolarized produce the interference pattern which is insensitive to rotation of in-plane optical axes of the DHFLC cell. We find that the field induced shift of the interference fringes can be described in terms of the electrically dependent Pancharatnam relative phase determined by the averaged phase shift, whereas the visibility of the fringes is solely dictated by the phase retardation.

PACS numbers: 61.30.Gd, 78.20.Jq, 42.70.Df, 42.79.Kr, 42.79.Hp

Keywords: helix deformed ferroelectric liquid crystal; subwavelength pitch; modulation of light.

## I. INTRODUCTION

Liquid crystal (LC) spatial light modulators (SLMs) are known to be the key elements widely employed to modulate amplitude, phase, or polarization of light waves in space and time [1]. Ferroelectric liquid crystals (FLCs) represent most promising chiral liquid crystal material which is characterized by very fast response time (a detailed description of FLCs can be found, e.g., in [2]). However, most of the FLC modes are not suitable for phase-only modulation devices because their optical axis sweeps in the plane of the cell substrate producing undesirable changes in the polarization state of the incident light.

In order to get around the optical axis switching problem the system consisting of a FLC half-wave plate sandwiched between two quarter-wave plates was suggested in [3]. But, in this system, the  $2\pi$  phase modulation requires the smectic tilt angle to be equal to  $45^\circ$ . This value is a real challenge for the material science and, in addition, the response time dramatically increases when the tilt angle grows up to  $45^\circ$  [4, 5].

An alternative approach proposed in [6, 7] is based on the orientational Kerr effect in a vertically aligned deformed helix ferroelectric LC (DHFLC) with subwavelength helix pitch. This effect is characterized by fast and, under certain conditions [8, 9], hysteresis-free electro-optics that preserves ellipticity of the incident light.

An important point is that all the above mentioned studies deal with the case of linearly polarized illumination where the incident beam is fully polarized. In this paper, we will go beyond this limitation and examine

the electro-optic behavior of the planar aligned DHFLC cells illuminated with unpolarized light as the way to obtain the response insensitive to the effect of electric-field-induced rotation of in-plane optical axes which was found to be responsible for the presence of amplitude modulation [10].

## II. EXPERIMENT

More specifically, we consider a DHFLC layer of thickness  $D$  with the  $z$  axis normal to the bounding surfaces:  $z = 0$  and  $z = D$ . The geometry of a uniformly lying DHFLC helix with subwavelength pitch where the helix (twisting) axis is directed along the  $x$  axis will be our primary concern.

According to Refs. [10–12], optical properties of such cells can be described by the effective dielectric tensor of a homogenized DHFLC helical structure. As is shown in Fig. 1, the zero-field ( $\mathbf{E} = 0$ ) dielectric tensor is uniaxially anisotropic with the optical axis directed along the twisting axis  $\hat{\mathbf{h}} = \hat{\mathbf{x}}$ . The zero-field effective refractive indices of extraordinary (ordinary) waves,  $n_h$  ( $n_p$ ), generally depend on the smectic tilt angle  $\theta$  and the optical (high frequency) dielectric constants characterizing the FLC material (see, e.g., equation (8) in Ref. [10] giving the expressions for  $\epsilon_h = n_h^2$  and  $\epsilon_p = n_p^2$ ).

Referring to Fig. 1, the electric-field-induced anisotropy is generally biaxial so that the dielectric tensor is characterized by the three generally different principal values (eigenvalues):  $\epsilon_{\pm} = n_{\pm}^2$  and  $\epsilon_z = n_z^2$ . The in-plane principal optical axes (eigenvectors)  $\hat{\mathbf{d}}_+ = \cos \psi_d \hat{\mathbf{x}} + \sin \psi_d \hat{\mathbf{y}}$  and  $\hat{\mathbf{d}}_- = \hat{\mathbf{z}} \times \hat{\mathbf{d}}_+$  are rotated about the vector of electric field,  $\mathbf{E} \parallel \hat{\mathbf{z}}$ , by the azimuthal angle  $\psi_d$ . In the low electric field region, the electric field dependence of the angle  $\psi_d$  is approximately linear:  $\psi_d \propto E$ , whereas the electrically induced part of the principal refractive indices,  $n_{\pm}$  and  $n_z$ , is typically

\* Email address: vladimir.ksaev@gmail.com

† Email address: epozhidaev@mail.ru

‡ Email address: alexei.d.kiselev@gmail.com

dominated by the Kerr-like nonlinear terms proportional to  $E^2$ . This effect — the so-called *orientational Kerr effect* — is caused by the electrically induced distortions of the helical structure. It is governed by the effective dielectric tensor of a nanostructured chiral smectic liquid crystal defined through averaging over the FLC orientational structure [6, 7, 11, 12].

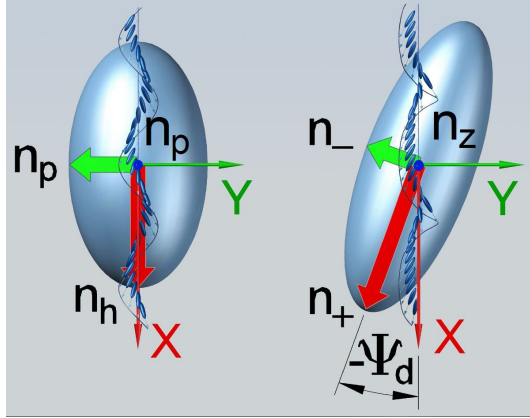


Figure 1: Ellipsoids of effective refractive indices of a short-pitch DHFLC cell. Left: at  $E = 0$ , the field-free effective ellipsoid is uniaxially anisotropic with the optical axis parallel to the helix axis (the  $x$  axis). Right: applying an electric field across the cell, makes the optical anisotropy biaxial with the two in-plane optical axes rotated by the angle  $\psi_d \propto E$  about the electric field vector  $\mathbf{E}$ .

In our experiments we have used the FLC mixture FLC-624 (from P.N. Lebedev Physical Institute of Russian Academy of Sciences) as the material for the DHFLC layer. The FLC-624 is a mixture of the FLC-618 (the chemical structure can be found in [7]) and the well-known nematic liquid crystal 5CB. The weight concentrations in the mixture are 98% of FLC-618 and 2% of 5CB. The phase transition sequence of the FLC-624 during heating from the solid crystalline phase is  $\text{Cr} \xrightarrow{+20^\circ\text{C}} \text{SmC}^* \xrightarrow{+60^\circ\text{C}} \text{SmA}^* \xrightarrow{+116^\circ\text{C}} \text{Iso}$ , whereas at cooling down from isotropic phase crystallization occurs around  $+6^\circ\text{C}$ . At room temperature ( $T = 23^\circ\text{C}$ ), the spontaneous polarization  $P_s$  and the FLC helix pitch  $p_0$  are  $185 \text{ nC/cm}^2$  and  $210 \text{ nm}$ , respectively.

The FLC-624 layer is sandwiched between two glass substrates covered by indium tin oxide (ITO) and aligning films with the thickness 20 nm and the gap is fixed by spacers at  $D \approx 53 \mu\text{m}$ . The FLC alignment technique that provides high-quality chevron-free planar alignment with smectic layers perpendicular to the substrates is detailed in [10].

Electro-optical studies of DHFLC cells are typically carried out by measuring the transmittance of normally incident light passing through crossed polarizers. By contrast, our experimental setup shown in Fig. 2 is based on a Mach-Zehnder two-beam interferometer where the FLC

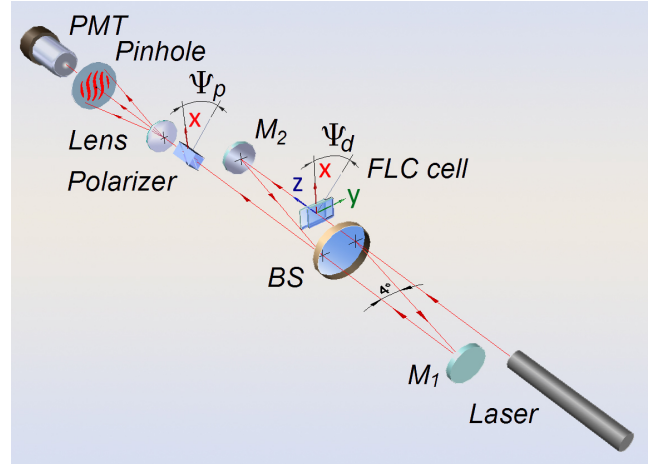


Figure 2: Experimental setup based on a Mach-Zehnder two-arm interferometer: BS is the beam splitter;  $M_1$  and  $M_2$  are the mirrors; PMT is the photomultiplier tube.

cell is placed in the path of the sample beam.

A helium-neon laser with the wavelength of 632.8 nm was used as a source of unpolarized light. A beam splitter (BS) divides a collimated unpolarized laser light into two beams, the reference and the sample beams, which, after reflection at the mirrors  $M_1$  and  $M_2$ , are recombined at the semireflecting surface of the beam splitter (BS). The interfering beams emerging from the interferometer optionally pass through an output polarizer with the transmission axis azimuth  $\psi_p$  and then are projected by the lens on to a screen with a pinhole. After passing the pinhole, light is collected by a photomultiplier (PMT) used in the linear regime as a photodetector.

The interferometer was adjusted to obtain the fringes of equal thickness shown in Fig. 2. The period of the interference pattern was 120 times larger than the pinhole diameter and thus our measurements of the light intensity were performed with an accuracy less than 0.7%. In order to minimize the polarizing effects of Fresnel reflections, all the directions of incidence were close to the normal (deviations from the normal were less than  $2^\circ$ ) so that the measured values of the degree of polarization of both beams were below  $10^{-4}$ .

In order to facilitate data processing for signals registered by PMT, the mirrors  $M_1$  and  $M_2$  were fine tuned so as to bring the pinhole into coincidence with the position of an intensity minimum of the field-free interference pattern. The experimental results measured for triangular wave-form of driving voltage with the frequency  $f = 50 \text{ Hz}$  (the voltage applied across the DHFLC cell ranges from  $-40 \text{ V}$  to  $+40 \text{ V}$ ) are shown in Figs. 4 and 5. These figures clearly indicate that the applied voltage results in modulation of the light intensity no matter whether the output wavefield passes through the polarizer or not. Another important effect is the electric field induced shift of the interference fringes which is illus-

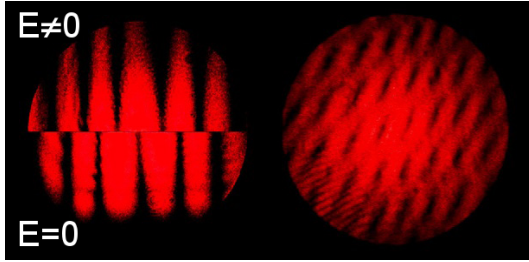


Figure 3: Left: The interference fringes at  $E \neq 0$  (top) and  $E = 0$  (bottom). Right: The interferogram obtained without the output polarizer shows the half-wave fringes.

trated in Fig. 3(left).

### III. THEORY

Theoretically, the above findings can be interpreted in terms of the output beam written as the sum of the vector amplitudes

$$\mathbf{E} = \mathbf{E}_s + \mathbf{E}_r \quad (1)$$

representing the light transmitted through the FLC cell (the sample beam),  $\mathbf{E}_s = \begin{pmatrix} E_x^{(s)} \\ E_y^{(s)} \end{pmatrix}$ , and the reference beam,  $\mathbf{E}_r = \begin{pmatrix} E_x^{(r)} \\ E_y^{(r)} \end{pmatrix} = \mathbf{T}_r \mathbf{E}_0 = e^{i\Phi_0} \mathbf{E}_0$ , where  $\mathbf{T}_r = e^{i\Phi_0} \mathbf{I}_2$  and  $\mathbf{I}_2$  is the  $2 \times 2$  unity matrix.

The vector amplitudes of incident and transmitted waves,  $\mathbf{E}_0$  and  $\mathbf{E}_s$ , are related through the standard input-output relation

$$\mathbf{E}_s = \mathbf{T}_s \mathbf{E}_0, \quad (2)$$

where  $\mathbf{T}_s$  is the transmission matrix that, for the case of normal incidence, can be easily obtained from the general results of Refs. [12, 13] in the form:

$$\mathbf{T}_s = \mathbf{Rt}(\psi_d) \begin{pmatrix} t_+ & 0 \\ 0 & t_- \end{pmatrix} \mathbf{Rt}(-\psi_d), \quad (3)$$

where  $\mathbf{Rt}(\psi_d) \equiv \begin{pmatrix} \cos \psi_d & -\sin \psi_d \\ \sin \psi_d & \cos \psi_d \end{pmatrix}$  is the rotation matrix,  $h = k_{\text{vac}} D$  is the thickness parameter and  $k_{\text{vac}} = \omega/c$  is the free-space wavenumber. Under certain conditions (see, e.g., discussion in [11]) the transmission coefficients,  $t_+$  and  $t_-$ , can be approximated by the well-known formulas

$$t_{\pm} \approx \exp(i\Phi_{\pm}), \quad \Phi_{\pm} = n_{\pm} h. \quad (4)$$

The beam emerging from the interferometer and the incident light are characterized by the  $2 \times 2$  equal-time

coherence matrices [14, 15],  $\mathbf{M}$  and  $\mathbf{M}_0$ , with the elements  $\mathbf{M}_{\alpha\beta} = \langle E_{\alpha} E_{\beta}^* \rangle$  and  $\mathbf{M}_{\alpha\beta}^{(0)} = \langle E_{\alpha}^{(0)} [E_{\beta}^{(0)}]^* \rangle$ , respectively. From the general relation linking these matrices  $\mathbf{M} = \mathbf{T} \mathbf{M}_0 \mathbf{T}^{\dagger}$ , where  $\mathbf{T} = \mathbf{T}_s + \mathbf{T}_r$  and a dagger (an asterisk) will indicate Hermitian (complex) conjugation, we have the coherence matrix of the output wavefield (1) given by

$$\mathbf{M} = \mathbf{M}_r + \mathbf{M}_s + \mathbf{M}_i, \quad \mathbf{M}_i = \mathbf{T}_s \mathbf{M}_0 \mathbf{T}_r^{\dagger} + \mathbf{T}_r \mathbf{M}_0 \mathbf{T}_s^{\dagger}, \quad (5)$$

where  $\mathbf{M}_r = \mathbf{T}_r \mathbf{M}_0 \mathbf{T}_r^{\dagger} = \mathbf{M}_0$  is the coherence matrix of the reference beam,  $\mathbf{M}_s = \mathbf{T}_s \mathbf{M}_0 \mathbf{T}_s^{\dagger}$  is the coherence matrix of the light transmitted through the DHFLC cell and  $\mathbf{M}_i$  is the interference term.

For the case where the input light is unpolarized and its coherency matrix is proportional to the unity matrix,  $\mathbf{M}_0 = \frac{I_0}{2} \mathbf{I}_2 \equiv \mathbf{M}_u$ , the coherence matrix (5) takes the form:

$$\frac{1}{I_0} \mathbf{M} = \frac{s_0}{2} \mathbf{I}_2 + \frac{s_p}{2} \begin{pmatrix} \cos 2\psi_d & \sin 2\psi_d \\ \sin 2\psi_d & -\cos 2\psi_d \end{pmatrix}, \quad (6)$$

$$I/I_0 \equiv s_0 = 1 + \frac{|t_+|^2 + |t_-|^2}{2} + \text{Re}[e^{-i\Phi_0}(t_+ + t_-)] \approx 2\{1 + \cos(\Phi - \Phi_0) \cos(\Delta\Phi/2)\}, \quad (7)$$

$$\Phi = (\Phi_+ + \Phi_-)/2, \quad \Delta\Phi = \Phi_+ - \Phi_-, \quad (8)$$

$$s_p = \frac{|t_+|^2 - |t_-|^2}{2} + \text{Re}[e^{-i\Phi_0}(t_+ - t_-)] \approx -2 \sin(\Phi - \Phi_0) \sin(\Delta\Phi/2), \quad (9)$$

where  $I = \langle \mathbf{E} \cdot \mathbf{E}^* \rangle$  is the total intensity of the beams exiting the interferometer;  $\Phi$  is the *averaged phase shift*;  $\Delta\Phi = (n_+ - n_-)h$  is the difference in optical path of the ordinary and extraordinary waves known as the *phase retardation*;

The approximate expressions for the *intensity and polarization parameters*,  $s_0$  and  $s_p$ , are derived using (4). This is the case where the matrix  $\mathbf{T}_s$  is unitary and, similar to the reference beam, the light field emerging from the FLC cell is unpolarized:  $\mathbf{M}_s = \mathbf{M}_r = \mathbf{M}_u$ . So, the only electric field dependent contribution to the coherence matrix of the total wavefield  $\mathbf{M}$  (see (5)) comes from the interference term  $\mathbf{M}_i$ .

This term is responsible for the following two effects: (a) electrically induced modulation of the intensity described by (7); and (b) the total wavefield (1) is partially polarized with the degree of polarization  $P = |s_p|/s_0$  and the Stokes parameters  $(S_1, S_2, S_3) = I_0 s_p (\cos 2\psi_d, \sin 2\psi_d, 0)$  varying with applied electric field. The latter, in particular, implies that the intensity of light that after the interferometer passes through a linear polarizer

$$I_p(\psi_p)/I_0 = [s_0 + s_p \cos 2(\psi_d - \psi_p)]/2 \quad (10)$$

depends on orientation of the polarizer transmission axis specified by the azimuthal angle  $\psi_p$ .

From (7), electric-field-induced modulation of the intensity does not depend on orientation of the optical axes (the azimuthal angle  $\psi_d$ ) and will occur even if the cell is optically isotropic and  $\Phi_+ = \Phi_- = \Phi$ . Interestingly, we can apply the interferometry based approach [16] to describe this effect in terms of the *Pancharatnam phase*,  $\Phi_P$ , which can naturally be defined as the phase generated by unitary evolution (transformation) of mixed polarization states (a recent discussion of the Pancharatnam phase for pure and mixed states in optics can be found, e.g., in [17, 18]). More specifically, in our case, the general relation

$$\text{Tr}[\mathbf{T}_s \mathbf{M}_0] = V \exp(i\Phi_P) \quad (11)$$

gives the Pancharatnam phase

$$\Phi_P = \begin{cases} \Phi, & \cos(\Delta\Phi/2) > 0 \\ \Phi + \pi, & \cos(\Delta\Phi/2) < 0 \end{cases} \quad (12)$$

and the *visibility* of the interference pattern

$$V = I_0 |\cos(\Delta\Phi/2)|. \quad (13)$$

The Pancharatnam phase (12) describes the relative phase between the beams before and after the cell (the phase between the mixed states  $\mathbf{M}_0$  and  $\mathbf{M}_s$ ) and is governed by the average of in-plane refractive indices:  $(n_+ + n_-)/2$ , whereas the visibility (13) is determined by the retardation phase  $\Delta\Phi$ . The intensity of the interference pattern (7) can now be recast into the simple form

$$I = \text{Tr} \mathbf{M} = 2[I_0 + V \cos(\Phi_P - \Phi_0)] \quad (14)$$

which is manifestly independent of optical axes orientation and shows that the electrically induced shift of the interferogram is solely dictated by the Pancharatnam phase.

Note that the points where the visibility vanishes ( $V = 0$ ) represent the phase singularities where the Pancharatnam phase is undefined. In the observation plane, such singularity points may, under certain conditions, form curves that can be visualized as the zero visibility fringes. From (13), such fringes indicate the loci of the points where the phase retardation meets the condition of half-wave plates:  $\cos(\Delta\Phi/2) = 0$ . So, these singularity lines might be called the *half-wave fringes*. Figure 3(right) shows the interferogram where such fringes arising from variations in cell thickness are easily discernible as zero-contrast stripes separating different areas of the interference fringes.

Formulas (7) and (10) can now be used to fit the data on electric field dependence of the light intensity measured by the PMT and presented in Figs. 4 and 5. It can be seen that the theoretical curves depicted as the solid lines are in good agreement with the experimental data.

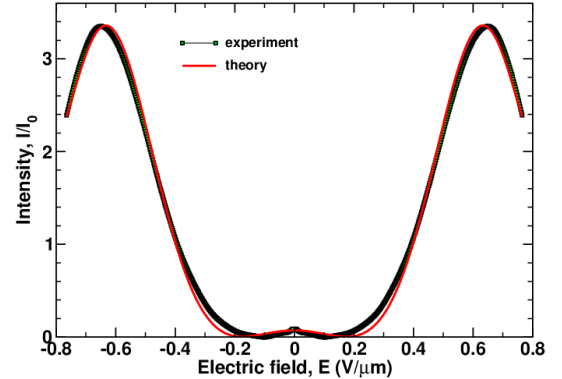


Figure 4: Intensity of output wavefield,  $I/I_0$ , as a function of the electric field for the DHFLC cell of thickness  $D \approx 53 \mu\text{m}$  filled with the FLC mixture FLC-624. Solid line represents the theoretical curve computed from (7) using the following parameters of the mixture:  $n_\perp \approx 1.5$  is the ordinary refractive index,  $n_\parallel \approx 1.71$  is the extraordinary refractive index,  $\theta \approx 33^\circ$  is the smectic tilt angle, and  $r_2 \approx 1.03$  is the biaxiality ratio.

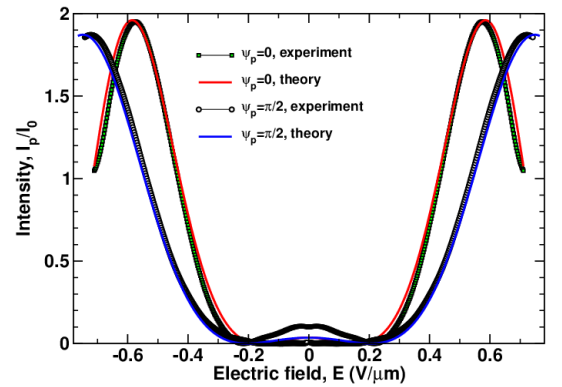


Figure 5: Intensity of output wavefield  $I_p/I_0$ , measured as a function of the electric field after the polarizer with the transmission axis oriented along ( $\psi_p = 0$ ) and perpendicular ( $\psi_p = \pi/2$ ) to the helix axis. Solid lines represent the theoretical curves computed from (10) using the parameters listed in the caption of Fig. 4.

#### IV. CONCLUSION

In conclusion, we have studied electric-field-induced modulation of unpolarized light in the DHFLC with sub-wavelength helix pitch using the experimental technique based on the Mach-Zehnder interferometer. Such modulation occurs under the action of the voltage applied across the cell and manifests itself in the electrically dependent shift and contrast of the interference pattern. The shift and the visibility are found to be governed by the Pancharatnam phase and the phase retardation, respectively. The distinctive features of the electro-optic response in the regime of unpolarized illumination are:

(a) insensitivity to the rotation of in-plane optical axes (this property was initially regarded as a requirement for pure phase modulation); and (b) modulation at subkilohertz operating frequencies (similar result was reported in [7] for vertically aligned DHFLCs). So, modulation of unpolarized light driven by the orientational Kerr effect might be of considerable importance for applications in photonic devices such as deflectors, switchable gratings

and wave-front correctors.

## ACKNOWLEDGMENTS

This work is supported by the RFBR grants 16-02-00441 A and 16-29-14012 ofi\_m. A.D.K. acknowledges partial financial support from the Government of the Russian Federation (Grant No. 074-U01).

---

[1] Uzi Efron, ed., *Spatial Light Modulator Technology: Materials, Applications, and Devices* (Marcell Dekker, NY, 1995) p. 665.

[2] Patrick Oswald and Paweł Pieranski, *Smectic and Columnar Liquid Crystals: Concepts and Physical Properties Illustrated by Experiments*, The Liquid Crystals Book Series (Taylor & Francis Group, London, 2006) p. 690.

[3] G. D. Love and R. Bhandari, “Optical properties of QHQ ferroelectric liquid crystal phase modulator,” *Opt. Commun.* **110**, 475–478 (1994).

[4] M. I. Barnik, V. A. Baikalov, V. G. Chigrinov, and E. P. Pozhidaev, “Electrooptics of a thin ferroelectric smectic  $C^*$  liquid crystal layer,” *Mol. Cryst. Liq. Cryst.* **143**, 101–112 (1987).

[5] E. P. Pozhidaev, M. A. Osipov, V. G. Chigrinov, V. A. Baikalov, L. M. Blinov, and L. A. Beresnev, “Rotational viscosity of the smectic  $C^*$  phase of ferroelectric liquid crystals,” *Zh. Eksp. Teor. Fiz.* **94**, 125–132 (1988).

[6] Evgeny P. Pozhidaev, Alexei D. Kiselev, Abhishek Kumar Srivastava, Vladimir G. Chigrinov, Hoi-Sing Kwok, and Maxim V. Minchenko, “Orientational Kerr effect and phase modulation of light in deformed-helix ferroelectric liquid crystals with subwavelength pitch,” *Phys. Rev. E* **87**, 052502 (2013).

[7] Evgeny P. Pozhidaev, Abhishek Kumar Srivastava, Alexei D. Kiselev, Vladimir G. Chigrinov, Valery V. Vashchenko, Alexander V. Krivoshey, Maxim V. Minchenko, and Hoi-Sing Kwok, “Enhanced orientational Kerr effect in vertically aligned deformed helix ferroelectric liquid crystals,” *Optics Letters* **39**, 2900–2903 (2014).

[8] L. M. Blinov, S. P. Palto, E. P. Pozhidaev, Yu. P. Bobylev, V. M. Shoshin, A. L. Andreev, F. V. Podgornov, and W. Haase, “High frequency hysteresis-free switching in thin layers smectic- $c^*$  ferroelectric liquid crystals,” *Phys. Rev. E* **71**, 071715 (2005).

[9] Eugene Pozhidaev, Vladimir Chigrinov, Anatoli Murauski, Vadim Molkin, Du Tao, and Hoi-Sing Kwok, “V-shaped electro-optical mode based on deformed-helix ferroelectric liquid crystal with subwavelength pitch,” *Journal of the SID* **20**, 273–278 (2012).

[10] Svetlana P. Kotova, Sergey A. Samagin, Evgeny P. Pozhidaev, and Alexei D. Kiselev, “Light modulation in planar aligned short-pitch deformed-helix ferroelectric liquid crystals,” *Phys. Rev. E* **92**, 062502 (2015).

[11] Alexei D. Kiselev, Eugene P. Pozhidaev, Vladimir G. Chigrinov, and Hoi-Sing Kwok, “Polarization-gratings approach to deformed-helix ferroelectric liquid crystals with subwavelength pitch,” *Phys. Rev. E* **83**, 031703 (2011).

[12] Alexei D. Kiselev and Vladimir G. Chigrinov, “Optics of short-pitch deformed-helix ferroelectric liquid crystals: Symmetries, exceptional points, and polarization-resolved angular patterns,” *Phys. Rev. E* **90**, 042504 (2014).

[13] A. D. Kiselev, R. G. Vovk, R. I. Egorov, and V. G. Chigrinov, “Polarization-resolved angular patterns of nematic liquid crystal cells: Topological events driven by incident light polarization,” *Phys. Rev. A* **78**, 033815 (2008).

[14] Leonard Mandel and Emil Wolf, *Optical Coherence and Quantum Optics* (Cambridge University Press, Cambridge, 1995) p. 1194.

[15] Christian Brosseau, *Fundamentals of Polarized Light: A Statistical Optics Approach* (Wiley, New York, 1998) p. 424.

[16] Erik Sjöqvist, Arun K. Pati, Artur Ekert, Jeeva S. Anandan, Marie Ericsson, Daniel K. L. Oi, and Vlatko Vedral, “Geometric phases for mixed states in interferometry,” *Phys. Rev. Lett.* **85**, 2845–2849 (2000).

[17] P. Hariharan, “The geometric phase,” *Progress in Optics* **48**, 293–363 (2005).

[18] D. Barberena, O. Ortíz, Y. Yugra, R. Caballero, and F. De Zela, “All-optical polarimetric generation of mixed-state single-photon geometric phases,” *Phys. Rev. A* **93**, 013805 (2016).